

Update of kaon semileptonic form factor using $N_f = 2 + 1$ PACS10 configurations

**Takeshi Yamazaki,^{a,b,*} Ken-ichi Ishikawa,^c Naruhito Ishizuka,^b
Yoshinobu Kuramashi,^b Yusuke Namekawa,^d Yusuke Taniguchi^b and
Naoya Ukita^a**

(PACS Collaboration)

^a*Institute of Pure and Applied Sciences, University of Tsukuba, Tsukuba, Ibaraki 305-8571, Japan*

^b*Center for Computational Sciences, University of Tsukuba, Tsukuba, Ibaraki 305-8577, Japan*

^c*Core of Research for the Energetic Universe, Graduate School of Advanced Science and Engineering, Hiroshima University, Higashi-Hiroshima, 739-8526, Japan*

^d*Education and Research Center for Artificial Intelligence and Data Innovation, Hiroshima University, Higashi-Hiroshima 739-8521, Japan*

E-mail: yamazaki@het.ph.tsukuba.ac.jp

We calculate the form factors for the kaon semileptonic decay process using the PACS10 configurations, whose physical volume is more than $(10 \text{ fm})^4$ very close to the physical point. The configurations were generated with the Iwasaki gauge action and $N_f = 2 + 1$ stout-smear non-perturbatively $O(a)$ -improved Wilson quark action at the three lattice spacings, 0.085, 0.063, and 0.041 fm. We present updated results for the form factors, and discuss their continuum extrapolations, momentum transfer interpolation, and short chiral extrapolation to tune the simulated pion and kaon masses to the physical ones. From the results with various analyses, the systematic error of the form factor at the zero momentum transfer is estimated. The value of $|V_{us}|$ is determined using our result, and is compared with those using the previous calculations and also those determined through the kaon leptonic decay process.

*The 41st International Symposium on Lattice Field Theory (LATTICE2024)
28 July - 3 August 2024
Liverpool, UK*

*Speaker

1. Introduction

The Cabibbo-Kobayashi-Maskawa (CKM) matrix elements in the first row give 2.2σ violation from the CKM unitarity [1]. It could suggest the existence of physics beyond the standard model. The value of the violation is essentially evaluated by $|V_{ud}|$ and $|V_{us}|$. The kaon leptonic ($K_{\ell 2}$) and semileptonic ($K_{\ell 3}$) decay processes are adopted to obtain the value of $|V_{us}|$, while it is reported that these values have a little tension [1]. To understand the violation of the CKM unitarity, it is important to investigate the difference between the two determinations of $|V_{us}|$.

For the $K_{\ell 2}$ decay determination, $|V_{us}|$ is basically given by the decay constant ratio F_K/F_π , which is well measured in the lattice QCD calculation. On the other hand, the $K_{\ell 3}$ form factor at the zero momentum transfer $f_+(0)$ is necessary to obtain $|V_{us}|$ for the $K_{\ell 3}$ determination. Since this calculation is more complicated than that of the decay constants, various studies have been carried out to obtain precise values of the $K_{\ell 3}$ form factor [2–11].

Using the $N_f = 2 + 1$ PACS10 configurations generated on huge volumes very close to the physical point, we also measured the $K_{\ell 3}$ form factor [12, 13] at the two larger lattice spacings. Although the accuracy of the result is comparable with the previous calculations, our result has a large systematic error coming from an estimate of the lattice spacing effect. To reduce the systematic error, we performed the calculation at the third lattice spacing [14]. In this report, we present updated results in our calculation from the last lattice conference, although all the results at the smallest lattice spacing are still preliminary. To obtain $f_+(0)$ from data of the $K_{\ell 3}$ form factors in finite momentum transfers at three lattice spacings, we perform a simultaneous fit for the momentum transfer interpolation, continuum extrapolation, and also short chiral extrapolation to the physical point. A systematic error of $f_+(0)$ for the continuum extrapolations is estimated by using various analyses. We also determine the value of $|V_{us}|$ using our preliminary result.

2. Simulation parameters

The PACS10 configurations were generated using the Iwasaki gauge action [15] and a non-perturbative $O(a)$ -improved Wilson quark action with the six-stout-smear link [16]. The simulation parameters of the PACS10 configurations at the three lattice spacings are tabulated in Table 1.

The same quark action is employed in the measurements for the two- and three-point functions for the $K_{\ell 3}$ form factors. The details of the calculation method in our study are described in Ref. [13].

Table 1: Simulation parameters of the PACS10 configurations at the three lattice spacings. The bare coupling (β), lattice size ($L^3 \cdot T$), physical spatial extent (L), lattice spacing (a), the number of the configurations (N_{conf}), pion and kaon masses (m_π , m_K), and the range of the timeslice separation (t_{sep}) between the source and sink operators in the three-point function are tabulated.

Label	β	$L^3 \cdot T$	L [fm]	a [fm]	N_{conf}	m_π [MeV]	m_K [MeV]	t_{sep} [fm]
PACS10/L128	2.20	256^4	10.5	0.041	20	142	514	3.4-3.9
PACS10/L160	2.00	160^4	10.1	0.063	20	138	505	2.3-4.1
PACS10/L256	1.82	128^4	10.9	0.085	20	135	497	3.1-4.0

Using the correlation functions, the matrix elements for the $K_{\ell 3}$ form factors are extracted, which are written by the two form factors $f_+(q^2)$ and $f_-(q^2)$ as,

$$\langle \pi(\vec{p}_\pi) | V_\mu | K(\vec{p}_K) \rangle = (p_K + p_\pi)_\mu f_+(q^2) + (p_K - p_\pi)_\mu f_-(q^2), \quad (1)$$

where V_μ is the weak vector current and q^2 is the momentum transfer squared. Another form factor $f_0(q^2)$ is defined with the two form factors as,

$$f_0(q^2) = f_+(q^2) + \frac{-q^2}{m_K^2 - m_\pi^2} f_-(q^2). \quad (2)$$

In this study, we calculate $f_+(q^2)$ and $f_0(q^2)$ with six and seven different q^2 , respectively, around $q^2 = 0$ at each lattice spacing.

For the calculation of the two- and three-point functions, we adopt the random source operator spread in the spin, color, and spatial spaces proposed in Ref. [17]. The exponentially smeared quark operator with the random source is also employed for the calculations of the correlation functions at the two smaller lattice spacings. The several time separations, t_{sep} , between the source and sink operators in the three-point function are utilized to investigate excited state contamination of the matrix elements. The range of t_{sep} at each lattice spacing is shown in Table 1. The form factors are evaluated with a combined analysis using the correlation functions with the two source operators and the different t_{sep} .

The periodic boundary condition is imposed in the spatial directions in the calculation of the correlation functions, while in the temporal direction the periodic and anti-periodic boundary conditions are employed. The average of the two-point correlation functions with the different boundary conditions makes the periodicity of the temporal direction effectively doubled. A similar average of the three-point functions suppresses the wrapping-around effect [18] in the small momentum region [12, 13].

Not only the local weak vector current but also the conserved vector one is employed to calculate the three-point functions to investigate finite lattice spacing effects in the form factors. The renormalization factor of the local vector current is determined from $Z_V = \sqrt{Z_V^\pi Z_V^K}$ where

$$Z_V^H = \frac{1}{F_H^{\text{bare}}(0)} \quad (3)$$

for $H = \pi, K$ with $F_H^{\text{bare}}(0)$ being the bare electromagnetic form factor evaluated using the local vector current at $q^2 = 0$.

3. Preliminary results

In this section our preliminary results for the $K_{\ell 3}$ form factors and also the value of $|V_{us}|$ determined from our results are presented.

3.1 $K_{\ell 3}$ form factors

Figure 1 shows our preliminary results for the $K_{\ell 3}$ form factors, $f_+(q^2)$ and $f_0(q^2)$, at $a = 0.041$ fm including the previous results in Ref. [13] using the renormalized local vector current. The data

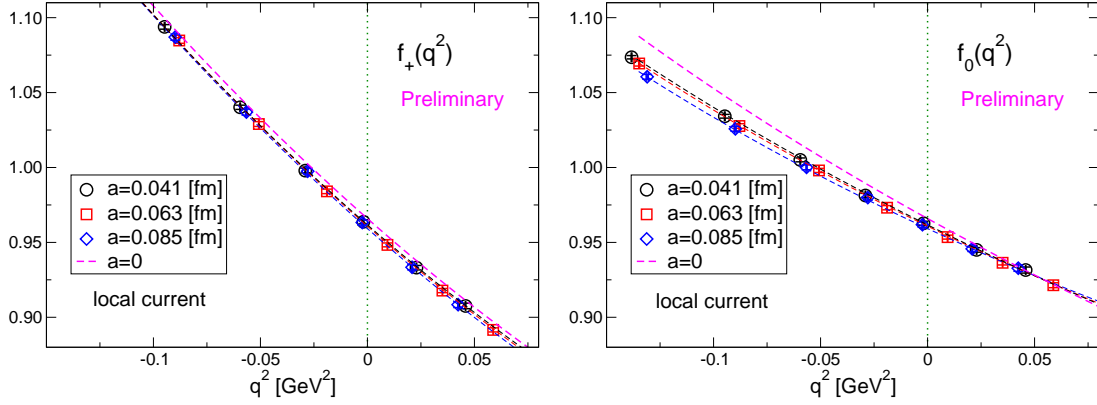


Figure 1: Lattice spacing dependences for $f_+(q^2)$ (left) and $f_0(q^2)$ (right) as a function of q^2 with the renormalized local vector current. The different symbols represent data at the different lattice spacings. The data at $a = 0.041$ fm are preliminary, while the other two data are presented in Ref. [13]. The dashed curves express the result of the simultaneous fit described in the text. The magenta curves correspond to the results in the continuum limit at the physical point.

for $f_+(q^2)$ and $f_0(q^2)$ are measured precisely at all the lattice spacings. Thanks to the huge volume of the PACS10 configurations, we can obtain several data near $q^2 = 0$ even using the periodic boundary condition in the spatial directions. The data with the conserved vector current have a similar quality to those for the local vector current.

To determine the value of $f_+(0)$, which is important to obtain $|V_{us}|$ through the $K_{\ell 3}$ decay, the data of the form factors are interpolated to $q^2 = 0$ and also extrapolated to $a = 0$ simultaneously. A fit form is based on the formulas at the next-to-leading order in the chiral perturbation theory [19, 20], and we add correction terms given by $(m_K^2 - m_\pi^2)^2$, q^2 , and lattice spacing effects. In the simultaneous fit, we use the data for $f_+(q^2)$ and $f_0(q^2)$ with both the local and conserved vector currents at all three lattice spacings. Figure 1 presents that the simultaneous fit works well in our local vector current data. The fit results at each lattice spacing are denoted by the curves in the same colors as the symbols. Since the simulated m_π and m_K are different from the physical ones, $m_{\pi^-} = 139.57061$ MeV and $m_{K^0} = 497.611$ MeV, as shown in Table 1, a short chiral extrapolation is carried out using the same formulas as in the simultaneous fit. The continuum limit results for $f_+(q^2)$ and $f_0(q^2)$ at the physical m_π and m_K are denoted by the magenta curves in the figure.

3.2 Continuum extrapolation of $f_+(0)$

The continuum extrapolation of $f_+(0)$ is discussed in this subsection, which corresponds to the simultaneous fit result at $q^2 = 0$ explained in the previous subsection.

Before discussing the continuum extrapolation, we present the effect of the chiral extrapolation in $f_+(0)$. The effect of the short chiral extrapolation for $f_+(0)$ is shown in the left panel of Fig. 2. At the three lattice spacing, the open circle and square symbols express the data at the simulated point with the local and conserved currents, respectively. The closed ones correspond to those at the physical point. It is noted that those data are estimated from q^2 interpolations at each lattice spacing for discussing the chiral and continuum extrapolations. The largest effect of the chiral extrapolation

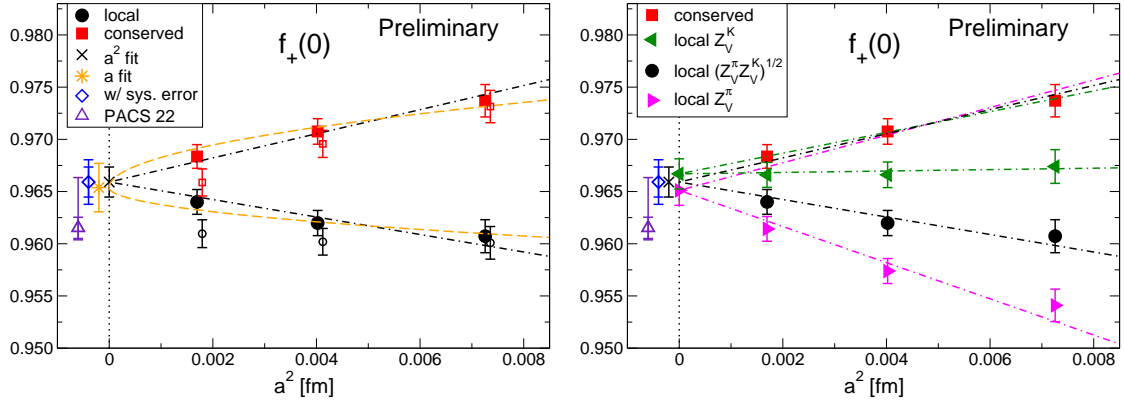


Figure 2: Left : Preliminary results of $f_+(0)$ at the physical point with the local (conserved) vector current denoted by black circle (red square) symbol as a function of a . The open circle and square symbols represent the results at the simulated meson masses. The dashed-dot and dashed curves express continuum extrapolations with quadratic and linear functions of a , respectively. The blue diamond and violet up triangle symbols express our preliminary and previous [13] results. The inner and outer errors express the statistical and total errors. The total error is evaluated by adding the statistical and systematic errors in quadrature. **Right :** The same figure as the left one, but includes the local vector current data with Z_V^π and Z_V^K denoted by magenta right and green left triangle symbols, respectively. The corresponding curves represent continuum extrapolations for those data with a quadratic function of a .

appears at the smallest lattice spacing. It is mainly caused by m_K , which differs from m_{K^0} by about 3% at the lattice spacing.

A continuum extrapolation of $f_+(0)$ in the simultaneous fit is expressed by black dashed-dot curves in the left panel of Fig. 2. In the fit form, the finite lattice spacing effect is expressed by a quadratic function of a , and we constrain that the two data with the local and conserved currents should coincide in the continuum limit. We also perform a fit with a linear function of a for the continuum extrapolation presented by orange dashed curves in the figure. The result is consistent with that from the a^2 extrapolation.

Various different analyses are performed to estimate systematic errors of $f_+(0)$. An example of the analyses is using a different renormalization factor in the local vector current data. As explained in the last section, the renormalization factor Z_V is determined from a combination of Z_V^π and Z_V^K in eq. (3). On the other hand, the renormalization factor can be determined from each Z_V^H . In a different analysis, the data with the local vector current are replaced by the same data but using a different renormalization factor, Z_V^π or Z_V^K . Those data are presented in the right panel of Fig. 2 with the magenta right and green left triangle symbols. The results in the continuum limit are well consistent with the black cross symbol which is the same one as in the left panel. Using results obtained from such different analyses, the systematic error of $f_+(0)$ is estimated from the maximum difference of the central value of the black cross result from those in the different analyses. The result with the total error including the systematic one is denoted by the blue diamond symbol in both the panels. The result reasonably agrees with our previous result in Ref. [13] denoted by the violet up triangle symbol in the panels.

For a more precise evaluation of $f_+(0)$, it is important to include the dynamical charm quark effect. We have started to generate $N_f = 2 + 1 + 1$ PACS10 configurations, named PACS10_c

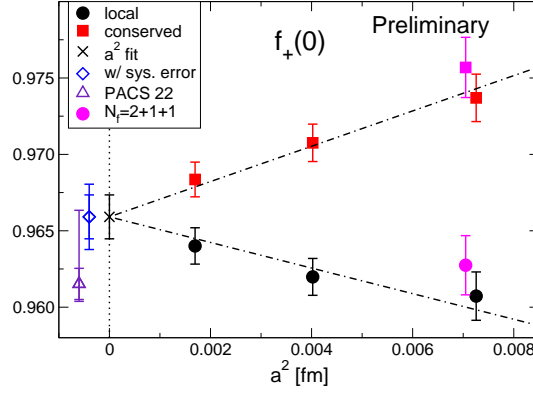


Figure 3: The same figure as Fig. 2, but contains the preliminary result from the PACS10_c configuration represented by magenta symbols.

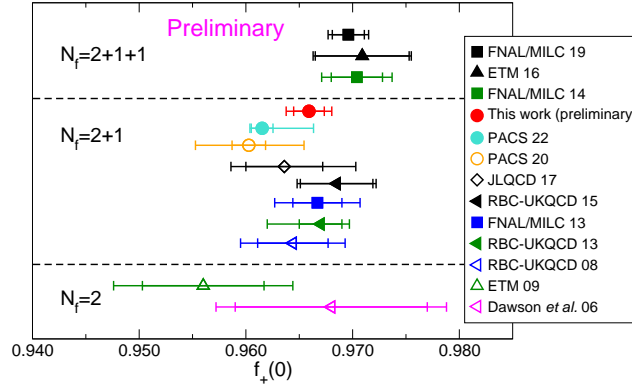


Figure 4: Comparison of our preliminary result of $f_+(0)$ with the previous results [2–13]. The inner and outer errors express the statistical and total errors. The total error is evaluated by adding the statistical and systematic errors in quadrature. The closed (open) symbols represent results in the continuum limit (at a finite lattice spacing).

configurations, which satisfy the same condition as the PACS10 configurations but contain the dynamical charm quark effect. So far only a preliminary result at the largest lattice spacing has been obtained. Figure 3 presents a reasonable agreement of the PACS10_c results with those from the $N_f = 2 + 1$ PACS10 configuration at a similar lattice spacing. While we will not discuss the result further in this report, we continue the calculation with PACS10_c configurations at smaller lattice spacings.

In Fig. 4, our preliminary result of $f_+(0)$ is compared with previous lattice calculations [2–11] including our previous results [12, 13]. The preliminary result in this work is consistent with those in our previous calculations, and also agrees with other lattice results within 2σ .

3.3 $|V_{us}|$ in the continuum limit

The value of $|V_{us}|$ is determined using the result of $f_+(0)$ discussed in the previous subsection with the experimental value $|V_{us}|f_+(0) = 0.21635(39)$ [21]. The obtained $|V_{us}|$ using our preliminary result is plotted in Fig. 5 together with the values using the previous lattice results [6, 8–13].

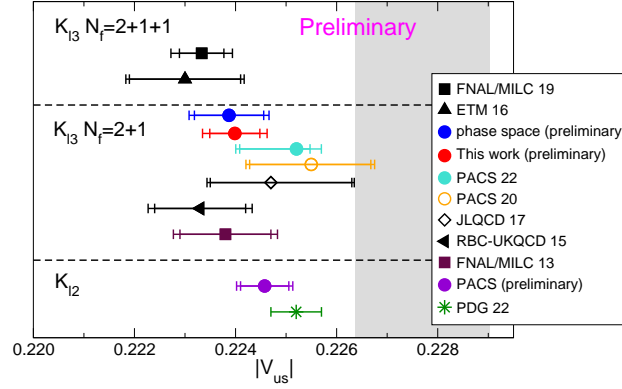


Figure 5: Comparison of $|V_{us}|$ using our preliminary result of $f_+(0)$ with the previous results [6, 8–13]. $|V_{us}|$ determined from the $K_{\ell 2}$ decay are also plotted using F_K/F_π of our preliminary result and PDG22 [1] together with the one obtained from the phase space integral with our results for $f_+(q^2)$ and $f_0(q^2)$. The closed (open) symbols represent results in the continuum limit (at a finite lattice spacing). The inner and outer errors express the lattice QCD and total errors. The total error is evaluated by adding the errors in the lattice QCD and experiment in quadrature. The value of $|V_{us}|$ determined from the unitarity of the CKM matrix using $|V_{ud}|$ in Ref. [24] is presented by the grey band.

Similar to the results of $f_+(0)$ in Fig. 4, our result is reasonably consistent with the other results through the $K_{\ell 3}$ determination.

Our result of $|V_{us}|$ from $f_+(0)$ also reasonably agrees with $|V_{us}|$ through the $K_{\ell 2}$ decay. In this determination, $|V_{us}|$ is obtained from the ratio of the decay constants F_K/F_π and the experimental value $|V_{us}|F_K/|V_{ud}|F_\pi = 0.27683(35)$ [22]. In Fig. 5, we plot $|V_{us}|$ with our preliminary value of F_K/F_π obtained from the $N_f = 2 + 1$ PACS10 configurations, and the one with F_K/F_π in PDG22 [1]. Furthermore, $|V_{us}|$ can be determined from the phase space integral [23] using our preliminary result of $f_+(q^2)$ and $f_0(q^2)$ in the continuum limit at the physical point. The values of $|V_{us}|$ obtained from the $K_{\ell 2}$ determination and phase space integral are consistent with that from $f_+(0)$ as presented in Fig. 5. On the other hand, $|V_{us}|$ estimated from the unitarity of the CKM matrix using the value of $|V_{ud}|$ in Ref. [24] is about 2σ away from our $K_{\ell 3}$ determination, which is shown by the grey band in the figure.

4. Summary

We have updated our calculation of the $K_{\ell 3}$ form factors using the three ensembles of the PACS10 configurations, which have more than $(10 \text{ fm})^4$ volumes very close to the physical point. The finite lattice spacing effect of $f_+(0)$ is examined using the data obtained from the local and conserved vector currents, and also using the different renormalization factors for the local vector current. The systematic error of our preliminary result of $f_+(0)$ is estimated from results with various different analyses. We have observed a reasonable agreement of our preliminary result of $f_+(0)$ with other lattice calculations. The value of $|V_{us}|$ determined with our $f_+(0)$ is reasonably consistent with those using other lattice results of $f_+(0)$, the $K_{\ell 2}$ decay determination, and from the phase space integral with our q^2 dependent form factors. In contrast to them, $|V_{us}|$ estimated from the CKM unitarity is different by about 2σ from our preliminary result.

For a more precise determination of $|V_{us}|$, an important future work is the inclusion of the dynamical charm quark effect. Toward this task, we have started to generate the $N_f = 2 + 1 + 1$ PACS10_c configurations. We have obtained a consistent result from the PACS10_c configuration with the PACS10 result at the largest lattice spacing. We will calculate the $K_{\ell 3}$ form factors at smaller lattice spacings with PACS10_c configurations.

Acknowledgments

Numerical calculations in this work were performed on Oakforest-PACS in Joint Center for Advanced High Performance Computing (JCAHPC) under Multidisciplinary Cooperative Research Program of Center for Computational Sciences, University of Tsukuba. This research also used computational resources of Oakforest-PACS by Information Technology Center of the University of Tokyo, the Type II subsystem on supercomputer "Flow" at Information Technology Center, Nagoya University, and of Fugaku by RIKEN CCS through the HPCI System Research Project (Project ID: hp170022, hp180051, hp180072, hp180126, hp190025, hp190081, hp200062, hp200167, hp210112, hp220079, hp230199, hp240207). The calculation employed OpenQCD system¹. This work was supported in part by Grants-in-Aid for Scientific Research from the Ministry of Education, Culture, Sports, Science and Technology (Nos. 19H01892, 23H01195, 23K25891) and MEXT as "Program for Promoting Researches on the Supercomputer Fugaku" (Search for physics beyond the standard model using large-scale lattice QCD simulation and development of AI technology toward next-generation lattice QCD; Grant Number JPMXP1020230409). This work was supported by the JLDG constructed over the SINET5 of NIL.

References

- [1] PARTICLE DATA GROUP collaboration, *Review of Particle Physics*, *PTEP* **2022** (2022) 083C01.
- [2] C. Dawson, T. Izubuchi, T. Kaneko, S. Sasaki and A. Soni, *Vector form factor in $K(13)$ semileptonic decay with two flavors of dynamical domain-wall quarks*, *Phys. Rev.* **D74** (2006) 114502 [[hep-ph/0607162](#)].
- [3] RBC-UKQCD collaboration, *$K(13)$ semileptonic form-factor from 2+1 flavour lattice QCD*, *Phys. Rev. Lett.* **100** (2008) 141601 [[0710.5136](#)].
- [4] ETM collaboration, *$K \rightarrow \pi l \nu$ Semileptonic Form Factors from Two-Flavor Lattice QCD*, *Phys. Rev.* **D80** (2009) 111502 [[0906.4728](#)].
- [5] FERMILAB LATTICE, MILC collaboration, *Kaon semileptonic vector form factor and determination of $|V_{us}|$ using staggered fermions*, *Phys. Rev.* **D87** (2013) 073012 [[1212.4993](#)].
- [6] RBC-UKQCD collaboration, *The kaon semileptonic form factor with near physical domain wall quarks*, *JHEP* **08** (2013) 132 [[1305.7217](#)].

¹<http://luscher.web.cern.ch/luscher/openQCD/>

- [7] FERMILAB LATTICE, MILC collaboration, *Determination of $|V_{us}|$ from a lattice-QCD calculation of the $K \rightarrow \pi \ell \nu$ semileptonic form factor with physical quark masses*, *Phys. Rev. Lett.* **112** (2014) 112001 [1312.1228].
- [8] RBC-UKQCD collaboration, *The kaon semileptonic form factor in $N_f = 2 + 1$ domain wall lattice QCD with physical light quark masses*, *JHEP* **06** (2015) 164 [1504.01692].
- [9] ETM collaboration, *$K \rightarrow \pi$ semileptonic form factors with $N_f = 2 + 1 + 1$ twisted mass fermions*, *Phys. Rev.* **D93** (2016) 114512 [1602.04113].
- [10] JLQCD collaboration, *Chiral behavior of $K \rightarrow \pi \ell \nu$ decay form factors in lattice QCD with exact chiral symmetry*, *Phys. Rev.* **D96** (2017) 034501 [1705.00884].
- [11] FERMILAB LATTICE, MILC collaboration, *$|V_{us}|$ from $K_{\ell 3}$ decay and four-flavor lattice QCD*, *Phys. Rev.* **D99** (2019) 114509 [1809.02827].
- [12] PACS collaboration, *K_{l3} form factors at the physical point on a $(10.9 \text{ fm})^3$ volume*, *Phys. Rev. D* **101** (2020) 094504 [1912.13127].
- [13] PACS collaboration, *$K_{\ell 3}$ form factors at the physical point: Toward the continuum limit*, *Phys. Rev. D* **106** (2022) 094501 [2206.08654].
- [14] PACS collaboration, *$|V_{us}|$ from kaon semileptonic form factor in $N_f = 2 + 1$ QCD at the physical point on $(10 \text{ fm})^4$* , *PoS LATTICE2023* (2024) 276 [2311.16755].
- [15] Y. Iwasaki, *Renormalization Group Analysis of Lattice Theories and Improved Lattice Action. II – four-dimensional non-abelian $SU(N)$ gauge model*, 1111.7054.
- [16] C. Morningstar and M.J. Peardon, *Analytic smearing of $SU(3)$ link variables in lattice QCD*, *Phys. Rev.* **D69** (2004) 054501 [hep-lat/0311018].
- [17] RBC-UKQCD collaboration, *The Pion’s electromagnetic form-factor at small momentum transfer in full lattice QCD*, *JHEP* **07** (2008) 112 [0804.3971].
- [18] PACS collaboration, *Electromagnetic pion form factor near physical point in $N_f = 2 + 1$ lattice QCD*, *PoS LATTICE2016* (2017) 160.
- [19] J. Gasser and H. Leutwyler, *Low-Energy Expansion of Meson Form-Factors*, *Nucl. Phys.* **B250** (1985) 517.
- [20] J. Gasser and H. Leutwyler, *Chiral Perturbation Theory: Expansions in the Mass of the Strange Quark*, *Nucl. Phys.* **B250** (1985) 465.
- [21] C.-Y. Seng, D. Galviz, W.J. Marciano and U.-G. Meißner, *Update on $|V_{us}|$ and $|V_{us}/V_{ud}|$ from semileptonic kaon and pion decays*, *Phys. Rev. D* **105** (2022) 013005 [2107.14708].
- [22] M. Di Carlo, D. Giusti, V. Lubicz, G. Martinelli, C.T. Sachrajda, F. Sanfilippo et al., *Light-meson leptonic decay rates in lattice QCD+QED*, *Phys. Rev.* **D100** (2019) 034514 [1904.08731].

- [23] H. Leutwyler and M. Roos, *Determination of the Elements $V(us)$ and $V(ud)$ of the Kobayashi-Maskawa Matrix*, *Z. Phys.* **C25** (1984) 91.
- [24] J.C. Hardy and I.S. Towner, *Superallowed $0^+ \rightarrow 0^+$ nuclear β decays: 2020 critical survey, with implications for V_{ud} and CKM unitarity*, *Phys. Rev. C* **102** (2020) 045501.